Inorg. Chem. **2009**, *48*, 3167−3176

Ferromagnetic Cu^{II}_4, Co^{II}_4, and Ni^{II}_6 Azido Complexes Derived from Metal-Assisted Methanolysis of Di-2,6-(2-pyridylcarbonyl)pyridine

Anastasia N. Georgopoulou,[†] Catherine P. Raptopoulou,[†] Vassilis Psycharis,[†] Rafael Ballesteros,[‡] Belén Abarca,[‡] and Athanassios K. Boudalis*,[†]

Institute of Materials Science, NCSR "Demokritos", 153 10 Aghia Paraskevi Attikis, Greece, and Departamento de Química Orgánica, Faculdad de Farmacia, Universidad de Valencia, Avda. Vicente Andrés Estellés s/n, 46100 Burjassot, Valencia, Spain

Received January 20, 2009

Reaction of copper(II) perchlorate with di-2,6-(2-pyridylcarbonyl)pyridine (pyCOpyCOpy, dpcp) in the presence of sodium azide yields complex $[Cu_4(N_3)_2\{pyC(OMe)(O)pyC(OMe)(O)py\}_2(MeOH)_2](ClO_4)\cdot 2MeOH$ (**1**·2MeOH), which crystallizes in the monoclinic $P2_1/c$ space group. Similar reaction of cobalt(II) nitrate yields complex $[Co_4(N_3)_2(NO_3)_2\{pyC(OMe)(O)pyC(OMe)(O)py\}_2]\cdot 0.5MeOH$ (**2**·0.5MeOH) which crystallizes in the monoclinic $I2/m$ space group. Reaction of nickel(II) perchlorate yields complex $[Ni_6(CO_3)(N_3)_6\{pyCOpyC(O)(OMe)py\}_3(MeOH)_2(H_2O)]$-$[Ni_6(CO_3)(N_3)_6\{pyCOpyC(O)(OMe)py\}_3\ (MeOH)_3](ClO_4)_2\cdot 1.8MeOH$ (**3**·1.8MeOH), which crystallizes in the triclinic $P\bar{1}$ space group, as a mixed salt of two similar Ni^{II}_6 cations, differing only in one terminally coordinated solvate molecule. The cation of **1** consists of four Cu^{II} ions in a rhombic topology, while complex **2** consists of four Co^{II} ions in a defective double cubane topology. Each of the two cations in **3** contains six Ni^{II} ions in a cyclic topology, adopting a chair conformation. In **1** and **2** the ligand has undergone complete methanolysis and full deprotonation, yielding its dianionic *bis-gem*-diol form. In **3** it has undergone only partial methanolysis. All complexes exhibit ferromagnetic intramolecular interactions. Ferromagnetism in **1** is caused by the structural constraints imposed by the $\{pyC(OMe)(O)pyC(OMe)(O)py\}^{2-}$ ligand on the Cu^{II} ions, while in the case of **2** and **3** it is the result of the combined effect of the end-on azido and alkoxo bridges of dpcp, which form $M-N_{azido}-M$ and $M-O_{alkoxo}-M$ angles between 90−105°. The magnetic susceptibility data of **1** and **3** were analyzed with appropriate spin Hamiltonian models ($\hat{H} = -2J_{ij}\hat{\mathbf{S}}_i\hat{\mathbf{S}}_j$ formalism). For **1**, a solution considering $J = +26.8$ cm^{-1} along the periphery of the rhombus was found. In **3** it was found that alternating exchange couplings of $J = +6.1$ cm^{-1} and $J' = +27$ cm^{-1} were operative along the periphery of the ring.

Introduction

Polynuclear transition metal complexes have been shown to exhibit several magnetic phenomena, interesting both from a fundamental and from an applications viewpoint; for example, Single-Molecule Magnetism (SMM)[1] and Quantum Tunneling of the Magnetization (QTM),[2] which have tested the limits of current models for magnetism of condensed matter. Besides their theoretical interest, these materials have been proposed as potential candidates for various technological applications,[3] like qubits for quantum computing,[4] coolants for magnetic refrigeration,[5] and MRI contrast agents.[6]

* To whom correspondence should be addressed. E-mail: tbou@ims.demokritos.gr. Phone: (+30) 210-6503346. Fax: (+30) 210-6503365.
† Institute of Materials Science, NCSR "Demokritos".
‡ Universidad de Valencia.

(1) (a) Christou, G.; Gatteschi, D.; Hendrickson, D. N.; Sessoli, R. *MRS Bull.* **2000**, *25*, 66–71. (b) Gatteschi, D.; Sessoli, R. *Angew. Chem., Int. Ed.* **2003**, *42*, 268–297.
(2) (a) Friedman, J. R.; Sarachik, M. P.; Tejada, J.; Ziolo, R. *Phys. Rev. Lett.* **1996**, *76*, 3830–3833. (b) Thomas, L.; Lionti, F.; Ballou, R.; Gatteschi, D.; Sessoli, R.; Barbara, B. *Nature* **1996**, *383*, 145–147.
(3) Boudalis, A. K.; Sanakis, Y.; Raptopoulou, C. P.; Psycharis, V. Magnetic phenomena in Zero-Dimensional Transition-Metal Spin-Clusters. In *Magnetism and Superconductivity in Low-Dimensional Systems: Utilization in Future Applications*; Nova Publishers: New York, 2008.
(4) (a) Leuenberger, M. N.; Loss, D. *Nature* **2001**, *410*, 789–793. (b) Hill, S.; Edwards, R. S.; Aliaga-Alcalde, N.; Christou, G. *Science* **2003**, *302*, 1015–1018. (c) Lehmann, J.; Gaita-Ariño, A.; Coronado, E.; Loss, D. *Nature Nanotechnology* **2007**, *2*, 312–317.
(5) Evangelisti, M.; Luis, F.; de Jongh, L. J.; Affronte, M. *J. Mater. Chem.* **2006**, *16*, 2534–2549.
(6) Cage, B.; Russek, S. E.; Shoemaker, R.; Barker, A. J.; Stoldt, C.; Ramachandaran, V.; Dalal, N. S. *Polyhedron* **2007**, *26*, 2413–2419.

10.1021/ic900115c CCC: $40.75
Published on Web 03/10/2009

Scheme 1. dpk and dpcp Ligands

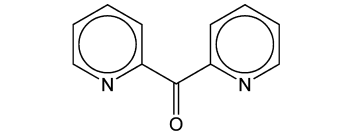

$(py)_2CO$, dpk

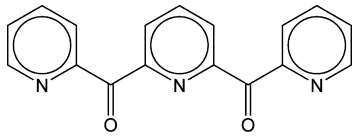

pyCOpyCOpy, dpcp

New ligands provide us with the opportunity to attain new structural types and spin topologies. Di-2-pyridyl ketone, (py_2CO, dpk, Scheme 1) has given access to a plethora of polynuclear transition metal complexes, from a variety of metal ions,[7] including a family of enneanuclear ferrous SMMs.[8] The origin of this interesting chemistry is the propensity of the carbonyl function of dpk to undergo metal-assisted solvolysis (alcoholysis in alcoholic solvents, or hydrolysis in non-alcoholic solvents) to yield a hemiacetal or a *gem*-diol; successive deprotonations of these forms generate anionic forms of the ligand with high coordinative versatility. We have previously shown that the related ligand di-2,6-(2-pyridylcarbonyl)pyridine (pyCOpyCOpy, dpcp, Scheme 1)[9] can yield a similar chemistry and provide access to polynuclear complexes. In our synthetic studies, we extensively explored the coordination chemistry of dpcp with metal acetates $M(O_2CMe)_2 \cdot xH_2O$ ($M^{II} = Co^{II}$, Cu^{II}, Ni^{II}), in various solvents, in the presence or in the absence of azides. We were thus able to crystallize and characterize complexes $[Co_{20}(OH)_6(O_2CMe)_{22}\{pyC(O)(OH)pyCO_2py\}_4(dmf)_2]$, (**I**),[10] $[Cu_5(O_2CMe)_6\{pyC(O)(OH)pyC(O)(OH)py\}_2]$(**II**),[11] $[Cu_4\{py(C(O)_2pyC(O)(OEt)py\}(O_2CMe)_5(EtOH)_2]$ (**III**),[12] $[Co_4\{py(C(O)(OMe)pyC(O)(OMe)py\}_2(O_2CMe)_2(N_3)_2]$ (**IV**),[12] and $[Ni_5\{pyCOpyC(O)(OMe)py\}_2(O_2CMe)_4(N_3)_4(MeOH)_2]$ (**V**)[13] confirming this ligand's potential for interesting new structures and spin topologies. Complexes **I** and **V** were found to exhibit slow magnetic relaxation.

Although the chemistry of dpcp with metal acetates proves to be very exiting, we were also interested in the products from reaction of dpcp with metal salts of weakly coordinating anions (i.e., nitrates, perchlorates) in the presence of azides, a known ferromagnetic coupler. Herein we report our first results from the coordination chemistry of dpcp with $M(ClO_4)_2 \cdot xH_2O$ and $M(NO_3)_2 \cdot xH_2O$ ($M^{II} = Cu^{II}$, Co^{II}, Ni^{II}) in MeOH, in the presence of NaN_3. In particular, complexes $[Cu_4\{pyC(OMe)(O)pyC(OMe)(O)py\}_2(N_3)_2(MeOH)_2](ClO_4)_2 \cdot 2MeOH$ (**1**·2MeOH), $[Co_4\{py(C(O)(OMe)pyC(O)(OMe)py\}_2(NO_3)_2(N_3)_2] \cdot 0.5MeOH$ (**2**·0.5MeOH), and $[Ni_6(CO_3)(N_3)_6\{pyCOpyC(O)(OMe)py\}_3(MeOH)_2(H_2O)][Ni_6(CO_3)(N_3)_6\{pyCOpyC(O)(OMe)py\}_3(MeOH)_3](ClO_4)_2 \cdot 1.8MeOH$ (**3**·1.8MeOH) were structurally characterized and magnetically studied.

Experimental Section

Materials. All materials were commercially available and used as received except dpcp, which was synthesized according to a literature procedure.[9] **Caution!** *Although no such tendency was observed during the present work, perchlorate and azide salts are potentially explosive and should be handled with care and in small quantities.*

Syntheses.$[Cu_4(N_3)_2\{pyC(OMe)(O)pyC(OMe)(O)py\}_2(MeOH)_2](ClO_4)_2 \cdot 2MeOH$ (1·2MeOH). Solid dpcp (20.0 mg, 0.069 mmol) was added to a solution of $Cu(ClO_4)_2 \cdot 6H_2O$ (102.0 mg, 0.276 mmol) in MeOH (35 mL). The solution changed from light blue to sky-blue and was stirred under reflux for 15 min. Solid NaN_3 (18 mg, 0.276 mmol) was then added to the solution, which was stirred under reflux for 5 min. During that time the color changed to light green. After cooling, the solution was left for slow evaporation. Green crystals of 1·2MeOH formed after 2 days. These were collected by decantation of the mother liquor, washed with 3 × 2 mL of cold MeOH, and dried in vacuo over silica gel. The yield was ∼29 mg (∼31% with respect to dpcp). The dried complex analyzed as solvent-free. Elemental analysis (%) calcd for $C_{40}H_{42}Cu_4Cl_2N_{12}O_{18}$: C 36.84, H 3.25, N 12.89; found C 36.91, H 3.30, N 12.82. IR (KBr disk): ν = 2073 (vs) [$\nu_{as}(N_3)$]; 1637 (m), 1605 (s), 1475 (m), 1460 (m) and 1441 (m) [ν(C···C)+ν(C···N)]; 1098 (vsb) [$\nu(ClO_4^-)$]; 758 (m) [$\delta(C-H)_{py}$]; 679 (m) [$\pi(C-H)_{py}$] cm^{-1}.

$[Co_4(N_3)_2(NO_3)_2\{pyC(OMe)(O)pyC(OMe)(O)py\}_2] \cdot 0.5MeOH$ (2·0.5MeOH). Solid dpcp (10.0 mg, 0.035 mmol) was added to a solution of $Co(NO_3)_2 \cdot 6H_2O$ (41.0 mg, 0.140 mmol) in MeOH (55 mL). The solution changed from light pink to pink and stirred under reflux for 15 min. Solid NaN_3 (9.0 mg, 0.140 mmol) was then added to the solution, which was stirred under reflux for 5 min, and the color changed to light orange-brown. After cooling, the solution was left for slow evaporation. Light brown crystals of **2**·0.5MeOH formed after ∼1 month. These were collected by decantation of the mother liquor, washed with 3 × 2 mL of cold MeOH, and dried in vacuo. The yield was ∼30 mg (∼52% with respect to dpcp). The dried complex was analyzed as solvent-free. Elemental analysis (%) calcd for $C_{38}H_{34}Co_4N_{14}O_{14}$: C 39.81, H 2.99, N 17.10; found C 39.90, H 3.04, N 17.05. IR (KBr disk): ν = 2073 (vs) [$\nu_{as}(N_3)$]; 1636 (m), 1603 (m), 1514 (s), 1466 (m) and 1441 (m) [ν(C···C)+ν(C···N)]; 1385 (s) [$\nu_d(NO)_{nitrate}$]; 1073 (s) [ν (C−O)$_{dpcp}$]; 762 (m) [$\delta(C-H)_{py}$]; 674 (m) [$\pi(C-H)_{py}$] cm^{-1}.

$[Ni_6(CO_3)(N_3)_6\{pyCOpyC(O)(OMe)py\}_3(MeOH)_2(H_2O)][Ni_6(CO_3)(N_3)_6\{pyCOpyC(O)(OMe)py\}_3(MeOH)_3](ClO_4)_2$ (3·1.8MeOH). Solid dpcp (20.0 mg, 0.069 mmol) was added to a solution of $Ni(ClO_4)_2 \cdot 6H_2O$ (101.0 mg, 0.276 mmol) in MeOH (35 mL). The solution changed from light green to green and stirred was under reflux for 15 min. Solid NaN_3 (18 mg, 0.276 mmol) was then added to the solution, which was stirred under reflux for 5 more min and the color changed to dark green. After cooling, the solution was layered with double the volume of Et_2O. Green needle-like crystals

(7) Papaefstathiou, G. S.; Perlepes, S. P. *Comments Inorg. Chem.* **2002**, *23*, 249–274.
(8) Boudalis, A. K.; Sanakis, Y.; Clemente-Juan, J. M.; Donnadieu, B.; Nastopoulos, V.; Mari, A.; Coppel, Y.; Tuchagues, J.-P.; Perlepes, S. P. *Chem.—Eur. J.* **2008**, *14*, 2514–2526.
(9) Abarca, B.; Ballesteros, R.; Elmasnaouy, M. *Tetrahedron* **1998**, *54*, 15287–15292.
(10) Boudalis, A. K.; Raptopoulou, C. P.; Abarca, B.; Ballesteros, R.; Chadlaoui, M.; Tuchagues, J.-P.; Terzis, A. *Angew. Chem., Int. Ed.* **2006**, *45*, 432–435.
(11) Boudalis, A. K.; Raptopoulou, C. P.; Psycharis, V.; Sanakis, Y.; Abarca, B.; Ballesteros, R.; Chadlaoui, M. *Dalton Trans.* **2007**, 3582–3589.
(12) Boudalis, A. K.; Raptopoulou, C. P.; Psycharis, V.; Abarca, B.; Ballesteros, R. *Eur. J. Inorg. Chem.* **2008**, 3796–3801.
(13) Boudalis, A. K.; Pissas, M.; Raptopoulou, C. P.; Psycharis, V.; Abarca, B.; Ballesteros, R. *Inorg. Chem.* **2008**, *47*, 10674–10681.

Table 1. Crystal Data for Complexes **1** and **2**

	1·2MeOH	**2**·0.5MeOH	**3**·1.8MeOH
formula	$C_{42}H_{50}Cl_2Cu_4N_{12}O_{20}$	$C_{38.5}H_{36}Co_4N_{14}O_{14.5}$	$C_{116.8}H_{113.2}Cl_2N_{54}Ni_{12}O_{39.8}$
FW	1368.00	1162.53	3685.63
T (K)	180(2)	180(2)	180(2)
crystal system	monoclinic	monoclinic	triclinic
space group	$P2_1/c$	$I2/m$	$P\bar{1}$
a (Å)	11.3132(2)	11.3290(2)	14.5652(2)
b (Å)	10.5766(1)	13.9776(2)	18.9292(3)
c (Å)	21.9862(4)	15.1100(3)	27.2138(4)
α (deg)			87.440(1)
β (deg)	90.241(1)	100.278(1)	84.744(1)
γ (deg)			85.770(1)
V (Å^3)	2630.74(7)	2354.31(7)	7445.72(19)
Z	2	2	2
ρ_{calc} (g cm^{-3})	1.727	1.640	1.644
λ (Å)	1.54180 (Cu Kα)	1.54180 (Cu Kα)	1.54180 (Cu Kα)
μ (mm^{-1})	3.522	11.546	2.730
refl. meas./unique	28638/4294 [R_{int} = 0.0195]	12882/2087 [R_{int} = 0.0752]	88627/20764 [R_{int} = 0.0811]
refl. obs. ($I > 2\sigma(I)$)	3968	2006	13192
parameters refined	461	221	2037
$R1$, $wR2$[a] (all)	$R1$ = 0.0300 $wR2$ = 0.0692	$R1$ = 0.0477 $wR2$ = 0.1231	$R1$ = 0.1140 $wR2$ = 0.2549
$R1$, $wR2$[a] (obs.)	$R1$ = 0.0272$wR2$ = 0.0669	$R1$ = 0.0462$wR2$ = 0.1216	$R1$ = 0.0786 $wR2$ = 0.2189

[a] $w = 1/[\sigma^2(F_o^2) + (aP)^2 + bP]$ and $P = (\max(F_o^2,0) + 2F_c^2)/3$; $R1 = \sum||F_o| - |F_c||/\sum|F_o|$ and $wR2 = \{\sum[w(F_o^2 - F_c^2)^2]/\sum w(F_o^2)^2\}^{1/2}$.

of (**3**·1.8MeOH) formed after 3 weeks. These were collected by decantation and dried in vacuo. The yield was ∼21 mg (∼17% with respect to dpcp). The dried complex was analyzed as solvent-free. Elemental analysis (%) calcd for $C_{115}H_{106}Cl_2N_{54}Ni_{12}O_{38}$: C 38.07, H 2.94, N 20.85; found: C 37.95, H 2.97, N 20.77. IR (KBr disk): ν = 2073 (vs) [$\nu_{as}(N_3)$]; 1672 (m) [$\nu(C{=}O_{dpcp})$]; 1591 (m), 1495 (s), 1475 (sh) and 1435 (m) [$\nu(C\cdots C)+\nu(C\cdots N)$]; 754 (m) [$\delta(C-H)_{py}$]; 680 (m) [$\pi(C-H)_{py}$] cm^{-1}.

X-ray Crystallography. A blue crystal of **1**·2MeOH (0.17 × 0.18 × 0.35 mm), a red crystal of **2**·0.5MeOH (0.23 × 0.25 × 0.37 mm), and a green crystal of **3**·1.8MeOH (0.11 × 0.12 × 0.70 mm) were taken directly from the mother liquor and immediately cooled to 180 K. Diffraction measurements were made on a Rigaku R-AXIS SPIDER Image Plate diffractometer using graphite monochromated Cu Kα radiation. Data collection (ω-scans) and processing (cell refinement, data reduction and Empirical absorption correction) were performed using the CrystalClear program package.[14] The structures were solved by direct methods using SHELXS-97[15] and refined by full-matrix least-squares techniques on F^2 with SHELXL-97.[16] Crystal data collection and refinement parameters are collected in Table 1. Further experimental crystallographic details for **1**·2MeOH: $2\theta_{max}$ = 130°; $(\Delta/\sigma)_{max}$ = 0.006; $(\Delta\rho)_{max}/(\Delta\rho)_{min}$ = 0.300/−0.278 e/Å^3. All hydrogen atoms were located by difference maps and were refined isotropically. All non-hydrogen atoms were refined anisotropically. Further experimental crystallographic details for **2**·0.5MeOH: $2\theta_{max}$ = 130°; $(\Delta/\sigma)_{max}$ = 0.000; $(\Delta\rho)_{max}/(\Delta\rho)_{min}$ = 0.561/−0.773 e/Å^3. All hydrogen atoms were located by difference maps and were refined isotropically; no H-atoms for the methanol solvate were included in the refinement. All non-hydrogen atoms were refined anisotropically. Further experimental crystallographic details for **3**·1.8MeOH: $2\theta_{max}$ = 118°; $(\Delta/\sigma)_{max}$ = 0.012; $(\Delta\rho)_{max}/(\Delta\rho)_{min}$ = 0.987/−0.726 e/Å^3. The hydrogen atoms of the ligands and the methyl hydrogens of the coordinated methanol molecules were introduced at calculated positions as riding on bonded atoms; the rest were not included in the refinement. All non-hydrogen atoms were refined anisotropically, except those of the methanol solvates which were refined isotropically. POV-Ray plots of **1**, **2**, and **3** were drawn using the Diamond 3 program package.

Physical Measurements. Elemental analysis for carbon, hydrogen, and nitrogen was performed on a PerkinElmer 2400/*II* automatic analyzer. Infrared spectra were recorded as KBr pellets in the range 4000−400 cm^{-1} on a Bruker Equinox 55/S FT-IR spectrophotometer. Variable-temperature magnetic susceptibility measurements were carried out on powdered samples in the 2−300 K temperature range using a Quantum Design MPMS SQUID susceptometer operating under magnetic fields of 0.1, 1, and 5 T for **1**, 0.1 T for **2**, and 1 T for **3**. Magnetization isotherms between 0 and 5.5 T were collected at 2 and 5 K for **1** and at 2 K for **2** and **3**. Diamagnetic corrections for the complexes were estimated from Pascal's constants. Alternating current (AC) magnetization experiments on **2** and **3** were carried out on a Quantum Design PPMS magnetometer. The magnetic susceptibilities for **1** and **3** have been computed by exact calculation of the energy levels associated with the spin Hamiltonian through diagonalization of the full matrix with the enhanced version of a general program for axial symmetry.[17] Least-squares fittings were accomplished with an adapted version of the function-minimization program MINUIT.[18] The error-factor R is defined as$R = \sum((\chi_{exp} - \chi_{calc})^2)/(N\chi^2_{exp})$, where N is the number of experimental points.

Results and Discussion

Syntheses. In our previous synthetic endeavors with dpcp, we tested its coordination chemistry with various metal(II) acetates, in particular cobalt(II), copper(II), and nickel(II). These salts were chosen for the coordinative versatility of the acetate ion, which is able to act as a bridging ligand, thus giving access to increased nuclearities. We were curious, however, about the products that could be obtained from the MX_2/pyCOpyCOpy/N_3^- reaction system in the absence of acetates, using metal salts of weaker coordinative potential,

(14) Rigaku/MSC. *CrystalClear*; Rigaku/MSC Inc.: The Woodlands, TX, 2005.
(15) Sheldrick, G. M. *SHELXS-97: Structure Solving Program*; University of Göttingen: Göttingen, Germany, 1997.
(16) Sheldrick, G. M. *SHELXL-97: Crystal Structure Refinement Program*; University of Göttingen, Göttingen, Germany, 1997.
(17) Clemente-Juan, J.-M.; Mackiewicz, C.; Verelst, M.; Dahan, F.; Bousseksou, A.; Sanakis, Y.; Tuchagues, J.-P. *Inorg. Chem.* **2002**, *41*, 1478–1491.
(18) James, F.; Roos, M. *Comput. Phys. Commun.* **1975**, *10*, 345; MINUIT Program, a System for Function Minimization and Analysis of the Parameters Errors and Correlations.

for example, $X^- = ClO_4^-$ or NO_3^-. We therefore tried reactions of copper(II), cobalt(II), and nickel(II) perchlorates and nitrates with dpcp in MeOH, in the presence of azides.

Reactions with copper(II) perchlorate yielded complex **1**. Its preparation reaction can be summarized in eq 1.

$$4Cu(ClO_4)_2 \cdot 6H_2O + 2pyCOpyCOpy + 2NaN_3 + 6MeOH \xrightarrow[\Delta]{MeOH} [Cu_4\{pyC(O)(OMe)pyC(O)(OMe)py\}_2(MeOH)_2(N_3)_2](ClO_4)_2 + 4HClO_4 + 2NaClO_4 + 24H_2O \quad (1)$$

On the other hand, reactions with copper(II) nitrate yielded no solid product, even at high concentrations. Slow evaporation of these solutions led to solids only when it was allowed to proceed to dryness. In that case, however, the solids were not crystalline.

Reactions with cobalt(II) perchlorate led to a crystalline product, whose IR spectrum revealed the presence of dpcp, azides, and perchlorates. However, no single crystals of adequate quality could be grown for structural characterization. Finally, reactions with cobalt(II) nitrate led to complex **2**. Its preparation reaction can be summarized in eq 2.

$$4Co(NO_3)_2 \cdot 6H_2O + 2pyCOpyCOpy + 2NaN_3 + 4MeOH \xrightarrow[\Delta]{MeOH} [Co_4\{pyC(O)(OMe)pyC(O)(OMe)py\}_2(NO_3)_2(N_3)_2] + 4HNO_3 + 2NaNO_3 + 24H_2O \quad (2)$$

Reactions with nickel(II) perchlorate led to complex **3**, containing a rare μ_6-carbonato bridge. X-ray crystallography revealed that complex **3** is actually obtained as a mixed salt of two cocrystallized cations of similar, but not identical, formulation. In particular, one is formulated as $[Ni_6(CO_3)(N_3)_6\{pyCOpyC(O)(OMe)py\}_3(MeOH)_2(H_2O)]^+$ and the other as $[Ni_6(CO_3)(N_3)_6\{pyCOpyC(O)(OMe)py\}_3(MeOH)_3]^+$. The source of the carbonate anion is considered to be atmospheric CO_2, which hydrolyzes in solution to carbonic acid. This is considered to be the reason for the relatively low yield of **3**; concentration of carbonates would be regulated by the atmospheric content in CO_2 and its solubility in the reaction mixture. Such bridging carboxylates have been observed in several cases.[19] Considering the former cation (**3A**), its formation reaction can be summarized by eq 3

$$6Ni(ClO_4)_2 \cdot 6H_2O + 3pyCOpyCOpy + 6NaN_3 + 5MeOH + CO_2 \xrightarrow[\Delta]{MeOH} [Ni_6(CO_3)(N_3)_6\{pyCOpyC(O)(OMe)py\}_3(MeOH)_2(H_2O)](ClO_4) + 5HClO_4 + 6NaClO_4 + 34H_2O \quad (3)$$

The reaction for the latter cation (**3B**) can be summarized by a similar equation. An interesting feature of **3** is that only one carbonyl function of dpcp has been methanolyzed. This behavior has previously been observed in the Ni^{II}_5 cluster **V**.[13]

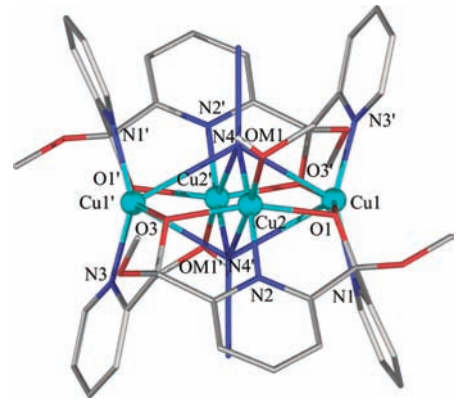

Figure 1. Partially labeled POV-Ray plot of the cation of **1**. For clarity, all H-atoms, except those of the hydroxyl function of the MeOH ligands, have been omitted. Symmetry operation symbols: $' = -x, 1 - y, -z$.

Description of Structures. The cation of complex **1**, shown in Figure 1, consists of four Cu atoms forming a rhombus, which resides on an inversion center. For the sake of brevity we will refer only to the asymmetric unit for our structural discussions, unless otherwise required. The first aspect of the structure that merits attention and should be analyzed before proceeding to the analysis of other structural aspects, concerns the azide ligand. For this ligand, we first recognize an interaction of clearly bonding character, that is, Cu(2)−N(4) (1.927 Å). In addition, we recognize the presence of longer bonds, suggesting weaker interactions, that is, Cu(2′)-N(4) (2.624 Å), Cu(1)−N(4) (2.807(2) Å), and Cu(1′)−N(4) (2.854(2) Å). Although the first is consistent with a Jahn−Teller elongated axial bonding distance, the two others are significantly longer and their character should be carefully evaluated. A survey of the Crystal Structure Database reveals that there are several examples of complexes comprising even more elongated Cu^{II}−azide bonds. Such bonds have been found in $[Cu_4(bpm)_2(N_3)_8]_n$ (2.868(2) and 2.967(2) Å; bpm = bis(pyrazol-1-yl)-methane),[20] $[Cu_2(terpy)_2(N_3)_4]$ (2.835 Å),[21] $[Cu_2(terpy)_2(N_3)_2(H_2O)_2](PF_6)_2$ (2.850 Å)),[22] $[Cu_2(L^2)_2(N_3)_2(ClO_4)_2]$, (2.950(5) Å; L^2 = 2-(3-(dimethylamino)propyliminomethyl)pyridine),[23] and $[Cu_2L_2(H_2O)(N_3)_4]_n$, (2.827 Å; L = 5-methylpyrimidin-2-amine).[24] Expanding our search criteria to other N-donor ligands, even longer bonds were found. On the basis of the above, we can assign these interactions to weak $Cu-N_{azide}$ bonds. Thus, the azides in complex **1** can be considered as adopting an asymmetric μ_4 end-on bridging mode. This is to be compared (Scheme 2) with the symmetric μ_4 end-on

(19) (a) Tong, M.-L.; Monfort, M.; Juan, J. M. C.; Chen, X.-M.; Bu, X.-H.; Ohba, M.; Kitagawa, S. *Chem. Commun.* **2005**, 233. (b) Graham, A.; Meier, S.; Parsons, S.; Winpenny, R. E. P. *Chem. Commun.* **2000**, 811. (c) Jiang, Y.; Wang, X.; Ying, X.; Zhong, F.; Cai, J.; He, K. *Inorg. Chem. Commun.* **2006**, *9*, 1063. (d) Cooper, G. J. T.; Newton, G. N.; Kogerler, P.; Long, D.-L.; Engelhardt, L.; Luban, M.; Cronin, L. *Angew. Chem., Int. Ed.* **2007**, *46*, 1340.

(20) Zhang, L.; Tang, L.-F.; Wang, Z.-H.; Du, M.; Julve, M.; Lloret, F.; Wang, J.-T. *Inorg. Chem.* **2001**, *40*, 3619–3622.

(21) Cortes, R.; Lezama, L.; Larramendi, J. I. R.; Insausti, M.; Folgado, J. V.; Madariaga, G.; Rojo, T. *J. Chem. Soc., Dalton Trans.* **1994**, 2573–2579.

(22) Cortes, R.; Urtiaga, M. K.; Lezama, L.; Larramendi, J. I. R.; Arriortua, M. I.; Rojo, T. *J. Chem. Soc., Dalton Trans.* **1993**, 3685–3694.

(23) Mukherjee, P. S.; Dalai, S.; Mostafa, G.; Lu, T.-H.; Rentschler, E.; Chaudhuri, N. R. *New J. Chem.* **2001**, *25*, 1203–1207.

(24) Song, X.-Y.; Li, W.; Li, L.-C.; Liao, D.-Z.; Jiang, Z.-H. *Inorg. Chem. Commun.* **2007**, *10*, 567–570.

Scheme 2. Left: Symmetric Bridging Mode of End-on μ_4-Azides in the $[M_9(N_3)_2(O_2CMe)_8\{(2\text{-py})CO_2\}_4]$ (M^{II} = Fe^{II}, Co^{II}, Ni^{II}) Family of Complexes. Right: Asymmetric Bridging Mode of End-on μ_4-Azides in **1**

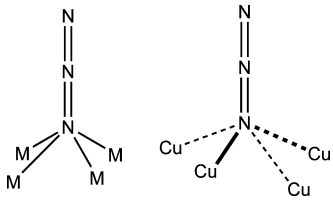

bridging mode having been observed in three other cases, in complexes $[M_9(N_3)_2(O_2CMe)_8\{(2\text{-py})CO_2\}_4]$ (M^{II} = Fe^{II}, Co^{II}, Ni^{II}; see ref 8 and references therein).

Thus, Cu(1) is hexacoordinate with a highly irregular coordination sphere that could be best described as a distorted tetragonal scalenohedron. Alternatively, we could describe it as bicapped square planar, experiencing a tetrahedral distortion. In that case, the tetrahedrally distorted square would be defined by donor atoms O(1)/O(3′)/N(1)/N(3′), whose distances from their mean plane are 0.451 (O(1)), 0.442 (O(3′)), −0.442 (N(1)) and −0.451 Å (N(3′)), while their distances from Cu(1) span a narrow range between 1.932−1.965 Å. Cu(2) is hexacoordinate, with an octahedral coordination exhibiting Jahn−Teller elongation. Its axial positions are occupied by O(M1) and N(4′), while its equatorial positions are occupied by O(1), N(2), O(3), and N(4).

Bridging between the four Cu atoms is achieved by the two $\{pyC(OMe)(O)pyC(OMe)(O)py\}^{2-}$ ligands through four alkoxo bridges, two from each ligand. Thus, each ligand is in effect μ_3-bridging. Additional bridging is supplied by two end-on bridging azides, as described above.

Complex **2**, shown in Figure 2, crystallizes in the monoclinic *I2/m* space group with one quarter of the molecule in the asymmetric unit. It consists of four Co atoms forming a defective double cubane. The molecule sits on an inversion center generated at the cross point of a 2-fold axis of symmetry passing through Co(2) and a mirror plane passing through Co(1), the atoms of the azide and nitrate ligands, as well as the atoms N(2) and C(9) of the dpcp ligand.

The structure of complex **2** is very similar to that of complex **IV** previously reported by us.[12] Their only difference is that the chelating acetate in complex **IV**, coming from cobalt(II) acetate, has now been replaced by a chelating nitrate, coming from cobalt(II) nitrate. Because of this similarity, we will not proceed to the full description of its structure.

Topologically speaking, the structures of **1** and **2** exhibit important similarities. In both complexes the metal core is planar and rhombic, with the azides forming polydentate end-on bridges almost normal to the mean M_4 plane (angles with the mean N_3 lines are 85.82 and 84.69°, respectively). Also the dpcp ligand in both complexes is present in its fully deprotonated *bis*-hemiacetal form, and adopts the same coordination mode (μ_3:η^1:η^1:η^1:η^2:η^2). The main difference resides in the fact that the terminal ligand in **1** (i.e., MeOH) is monodentate, while the terminal ligand in **2** (i.e., $MeCO_2^-$) is chelating, thus occupying

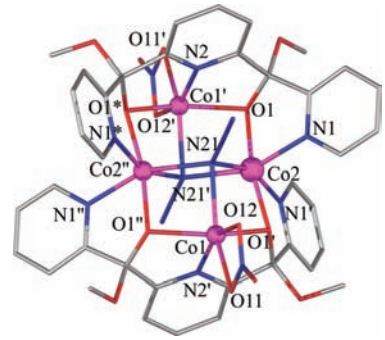

Figure 2. Partially labeled POV-Ray plot of **2**. For clarity, all H-atoms have been omitted. Symmetry operation symbols: ′ = −*x*, *y*, −*z*, ″ = −*x*, −*y*, −*z*, * = *x*, −*y*, *z*.

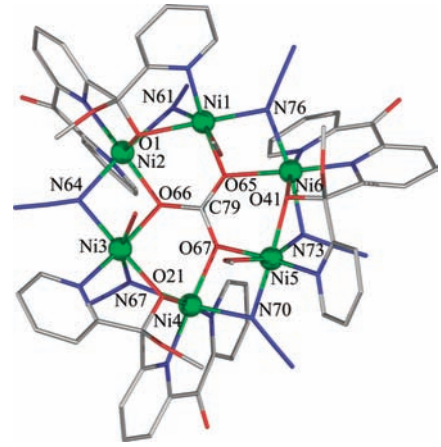

Figure 3. Partially labeled POV-Ray plot of cation **3A**. For clarity, all hydrogen atoms have been omitted.

an additional coordination position, which is unavailable for azide coordination. Accordingly, the non-bonding M−N distance in **2** is too large (3.42 Å) for any type of bond to be possible. Thus, the two complexes are topologically very similar (with the absence of a $Co-N_{azide}$ bond in **2**), although their geometric parameters differ significantly.

Complex **3**, shown in Figure 3, crystallizes in the $P\bar{1}$ space group and consists of two independent hexanuclear molecular cations. Though structurally very similar, these cations are not identical, differing in their terminal coordinated solvate molecules. Cation **3A**, $[Ni_6(CO_3)(N_3)_6\{pyCOpyC(O)(OMe)py\}_3(MeOH)_2(H_2O)]^+$ contains two terminal methanol ligands and one aquo ligand, while cation **3B**, $[Ni_6(CO_3)(N_3)_6\{pyCOpyC(O)(OMe)py\}_3(MeOH)_3]^+$, contains three terminal methanol ligands. Because of the structural similarity of the two molecules, we will only describe cation **3A**, unless otherwise required. The six Ni^{II} ions in **3** are arranged in a cyclic topology, adopting a chair conformation (Figure 4). The most salient feature of the structure of **3** is the μ_6-carbonate bridge situated near the center of the Ni_6 core. This feature, although rare, is not unique, having been observed in other Ni^{II} clusters.[19] Its assignment as a CO_3^{2-} ion (and not as a NO_3^- one) was based on combined consideration of charge-balance requirements (a −2 charge was required) and the contents of the reaction system (no nitrates were present in the reactants).

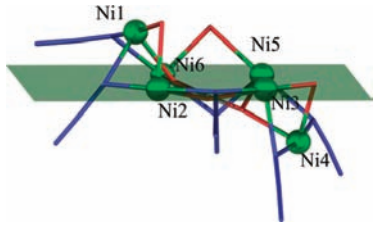

Figure 4. Side view of the Ni^{II}_6 core in **3A**, showing its chair conformation; the least-squares plane is defined by Ni(2), Ni(3), Ni(5), and Ni(6).

All Ni atoms in **3** are hexacoordinate, exhibiting distorted octahedral coordination geometries. However, they are subdivided into two types, each occurring alternately along the Ni_6 ring. The first type (Ni(1), Ni(3), and Ni(5)) exhibits a N_3O_3 donor atom set, while the second type (Ni(2), Ni(4), and Ni(6)) exhibits a N_2O_4 one. The dpcp molecules in **3** are in their carbonyl-hemiacetal form, with only one carbonyl function having been methanolyzed. Each dpcp ligand bridges two nickel atoms in a $\mu:\eta^1:\eta^1:\eta^1:\eta^2$ fashion. Additional bridging is provided by the carbonate ligand, adopting a $\mu_6:\eta^2:\eta^2:\eta^2$ bridging mode, and by six end-on azides. However, bridging along the Ni_6 ring is not uniform and is observed in two alternating types. The first type (observed between Ni(1)−Ni(2), Ni(3)−Ni(4), and Ni(5)−Ni(6)) comprises one end-on azide and one alkoxo monatomic O-bridge, provided by the dpcp ligand; the second type (observed between Ni(2)−Ni(3), Ni(4)−Ni(5), and Ni(6)−Ni(1)), comprises one end-on azide and one carbonato monatomic O-bridge. This difference is illustrated by the structural parameters of the bridging moieties; average Ni···Ni separations are of 3.030 Å for the former type and of 3.277 Å for the latter. Similarly, average $Ni-N_{azide}-Ni$ angles are of 92.24 and 101.77°, respectively. Finally, the average $Ni-O_{alkoxo}-Ni$ angle of the former bridge type is 93.30°, while the average $Ni-O_{carbonato}-Ni$ angle of the latter bridge type is 104.36°.

The six Ni atoms are found in a chair conformation as shown by the side-view of the core of **3A** (Figure 4). Atoms Ni(2), Ni(3), Ni(5), and Ni(6) are roughly coplanar, with Ni(1) and Ni(4) deviating from their mean plane by 1.521 and −1.783 Å, respectively.

The structure of **3** bears strong similarities with that of complex $\{K\subset[Ni_6(CO_3)(N_3)_6(O_2CMe)_3(dpkMeCN\text{-}H)_3]\}_2[K_2(H_2O)_2]$,[19a] which also consists of two Ni_6 rings, each containing a μ_6-carbonato bridge and six end-on μ-azides. The similarities expand to the dpk ligand, present in its cyanomathylated form, which may be viewed as the prototype of the dpcp ligand studied in this work; also to the alternating types of Ni−Ni pairs, one containing an alkoxo monatomic O-bridge from the dpk ligand and the other containing a carbonato O-bridge. However, the difference from **3** is that its core is practically planar, in contrast to the chair conformation of the core in **3**.

Magnetic Properties. Magnetic Properties of Complex 1. The $\chi_M T$ product for **1** is 1.82 $cm^3\ mol^{-1}$ K, above the value predicted for four non-interacting $S = 1/2$ ions (1.65 $cm^3\ mol^{-1}$ K, $g = 2.1$), suggesting ferromagnetic interactions (Figure 5). This is corroborated by the increase of $\chi_M T$ upon cooling, up to a maximum of 3.37 $cm^3\ mol^{-1}$ K at 9 K (1 T). Further cooling under a 1 T field leads to a sharp drop of $\chi_M T$ to 2.77 $cm^3\ mol^{-1}$ K at 2 K. To ascertain whether this drop is associated with antiferromagnetic interactions, or Zeeman splitting inside the magnetic field, multifield data were collected for **1**. These data showed that the observed maximum is field dependent and is suppressed upon field increase, while also moving to higher temperatures. Under a 5 T field the maximum appears at 20 K (3.16 $cm^3\ mol^{-1}$ K), while under a 0.1 T field it disappears, giving its place to a plateau of 3.44 $cm^3\ mol^{-1}$ K below 5 K, a value agreeing well with an $S = 2$ spin ($g = 2.14$). This behavior could be nicely modeled by considering the Zeeman interactions inside the magnetic field, with no antiferromagnetic interactions, intra- or intermolecular, being required (see below).

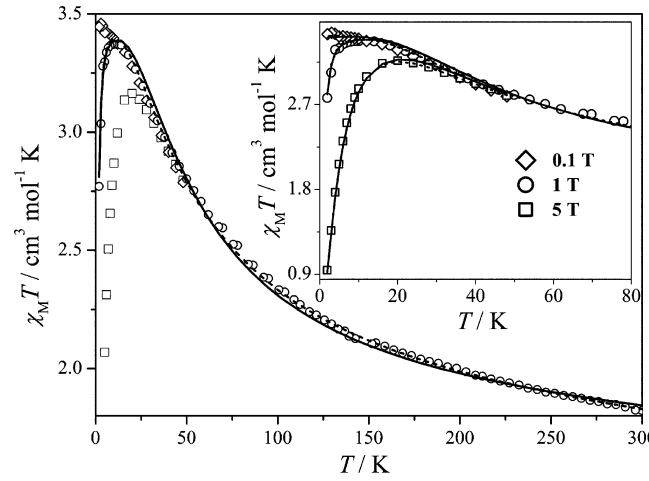

Figure 5. $\chi_M T$ vs T data for complex **1** under magnetic fields of 0.1 (◇), 1(○), and 5 (□) T. The lines represent the best-fit solutions **A** (solid) and **C** (dashed), according to the model discussed in the text. For clarity, only the 1 T calculated curve is shown over the whole temperature range. The inset shows an expansion of the 2−80 K region with the calculated curves for all fields.

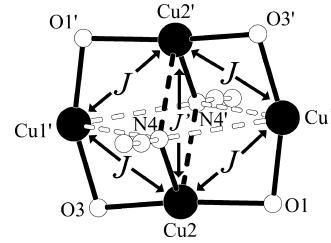

Figure 6. Spin-coupling scheme for **1**.

The symmetry of **1**, as revealed by its crystal structure, allows us to consider one coupling parameter for all exchange interactions between adjacent Cu^{II} ions along the periphery of the rhombus (see Figure 6). In addition, the end-on bridging azide could justify the consideration of an additional diagonal exchange interaction, between Cu(2) and Cu(2′). A similar interaction between Cu(1) and Cu(1′) is considered to be highly unlikely, in view of the large respective Cu−N distances. To account for the behavior of **1** under different magnetic fields, the Zeeman interaction was introduced into our Hamiltonian. Thus, the spin Hamiltonian used was

$$\hat{H} = -2[J(\hat{\mathbf{S}}_1\hat{\mathbf{S}}_2 + \hat{\mathbf{S}}_2\hat{\mathbf{S}}_{1'} + \hat{\mathbf{S}}_1\hat{\mathbf{S}}_{2'} + \hat{\mathbf{S}}_{2'}\hat{\mathbf{S}}_1) + J'\hat{\mathbf{S}}_2\hat{\mathbf{S}}_{2'}] + \beta g\mathbf{H}\sum_{i=1}^{4}\hat{\mathbf{S}}_i \quad (4)$$

Initial fits were carried out by considering $J' = 0$ and yielded a solution with best-fit parameters $J = +26.8$ cm^{-1}, $g = 2.135$, and $R = 1.4 \times 10^{-4}$ (Solution **A**). To improve on this result, the parameter J' was allowed to vary. From the exploration of the parameter space of the problem, two solutions were derived, their best-fit parameters being as follows: $J = +16.0$ cm^{-1}, $J' = +51.8$ cm^{-1}, $g = 2.143$, and $R = 5.9 \times 10^{-5}$ (Solution **B**) and $J = +35.6$ cm^{-1}, $J' = -15.0$ cm^{-1}, $g = 2.140$, and $R = 6.5 \times 10^{-5}$ (Solution **C**). An error-contour plot (Figure 7) revealed them as being the only local minima for a 2*J* model. These solutions do offer a substantial improvement to the agreement with the experimental data, with the *R* factor being decreased to half its value, compared to solution **A**. Considering, however, that this is to be expected by the addition of an extra fitting parameter, the physical meaning of these solutions was examined by consideration of the structural parameters of **1** (see Magnetostructural Correlations).

Magnetostructural Correlations. To carry out qualitative magnetostructural correlations in **1** without the need of complicated theoretical techniques, we have to choose a simplified description for the coordination geometry of Cu(1), that is, that of a tetrahedrally distorted square planar one. Although this is not entirely precise (see Description of Structures), it is a necessary assumption to simplify our problem. Moreover, from a magnetic point of view, it provides an interpretation in perfect agreement with our experimental results.

According to this assumption, the magnetic orbitals of Cu(1) will be those pointing toward donor atoms O(1), O(M1), O(3), and N(4′), which we assume to define a tetrahedrally distorted square. Although they are not expected to be fully of $d_{x^2-y^2}$ character, we assume that they are nevertheless the magnetic orbitals for that atom. We may first note that from the results of our fits, *J* has been invariably found to correspond to a ferromagnetic interaction. We should also point to the fact that the only superexchange pathways along the periphery of the rhombus, that pass through magnetic orbitals of Cu(1) and Cu(2), are the alkoxo O atoms O(1) and O(3). From these two observations we conclude that ferromagnetism in **1** is transmitted through the alkoxo atoms of the dpcp ligand. This can be rationalized by the Cu(1)−O(1)−Cu(2) angle (97.011(60)°) which is expected to decrease the antiferromagnetic component of magnetic exchange between the magnetic orbitals of Cu(1) and Cu(2). In addition, the dihedral angle of the mean planes containing the magnetic orbitals of Cu(1) and Cu(2) (mean planes O(1)/O(M1)/O(3)/N(4′) and O(1)/O(3′)/N(1)/N(3′), respectively) will affect the strength and sign of this exchange. This angle being 88.691(57)°, we can conclude that this is an additional structural factor that favors ferromagnetic exchange, by increasing the orthogonality between the magnetic orbitals of the two metal centers.

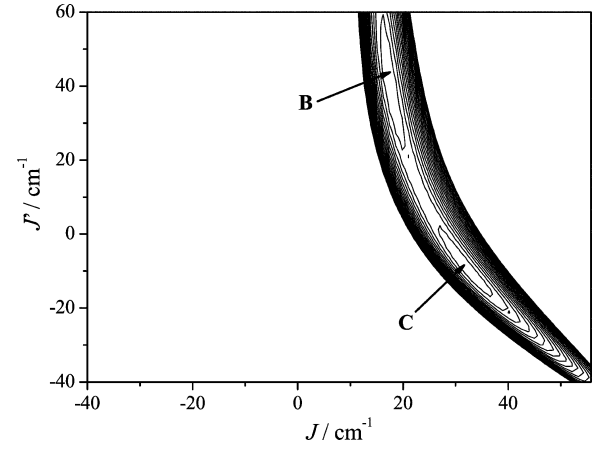

Figure 7. Error-contour plot of J' vs J showing the solutions **B** and **C** as local minima.

Similar reasoning is required to decide which of the solutions **A**−**C** is more realistic, that is, which J' value is physically more meaningful. As previously discussed (see Description of Structures) the azido bridges are asymmetric; for example, N(4) occupies an equatorial position of Cu(2) and an axial position of Cu(2′). Thus, any magnetic exchange will be transmitted through the magnetic orbitals of one Cu^{II} ion (equatorial position) and the non-magnetic orbitals of the other (axial position). It is therefore expected that the magnetic exchange will not be particularly strong. In addition the relatively large Cu(2)−N(4)−Cu(2′) angle (103.10°) is not expected to favor the appearance of ferromagnetic exchange. Ruiz et al.,[25] based on hybrid density-functional calculations, found that for the model complex $[Cu_2(N_3)_2(en)_2]^{2+}$ magnetic couplings switch from ferro- to antiferromagnetic for Cu−N_{azide}−Cu angles above 104°. Also, in a previous study, we determined a coupling of −36 cm^{-1} for a Cu−N_{azide}−Cu angle of 104.3°.[26] The Cu(2)−N(4)−Cu(2′) angle in **1** is very close to these critical values, thus supporting the conclusion of a very weak antiferromagnetic coupling. Therefore, on these grounds we choose to disregard solution **B**, which entails a strongly ferromagnetic Cu(2)−Cu(2′) interaction. However, based on the quality of the fits alone, we cannot safely decide between solutions **A** ($J' = 0$) or **C** ($J' = -15$ cm^{-1}), since improvements of the fits are normally expected upon introduction of additional variables. Although we are inclined to favor solution **A**, as the one considering the smallest number of fitting parameters, a diagonal interaction (J') cannot be excluded. However, we are confident that any such interaction, if operative, should be weak (minimum *J* value, −15 cm^{-1}) and antiferromagnetic.

Further verification of our conclusions comes from magnetization isotherms collected at low temperatures. For both solutions **A** and **C**, a well isolated $S = 2$ ground state is derived, with a first excited $S = 1$ state at 53.6 and 41.3 cm^{-1}, respectively. The magnetization isotherms collected at 2 and 5 K are perfectly simulated by Brillouin curves,

(25) Ruiz, E.; Cano, J.; Alvarez, S.; Alemany, P. *J. Am. Chem. Soc.* **1998**, *120*, 11122.
(26) Saha, S.; Koner, S.; Tuchagues, J.-P.; Boudalis, A. K.; Okamoto, K.-I.; Banerjee, S.; Mal, D. *Inorg. Chem.* **2005**, *44*, 6379.

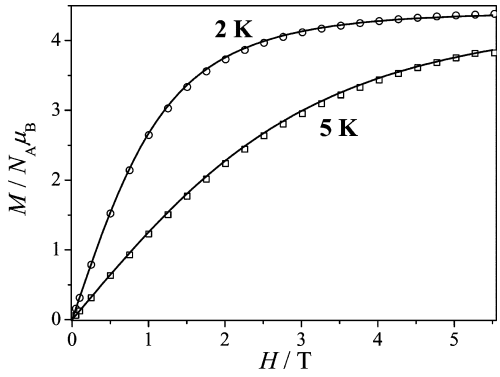

Figure 8. Magnetization isotherms of **1** at 2 (○) and 5 (□) K. The solid lines represent Brillouin curves assuming $S = 2$ and $g = 2.2$.

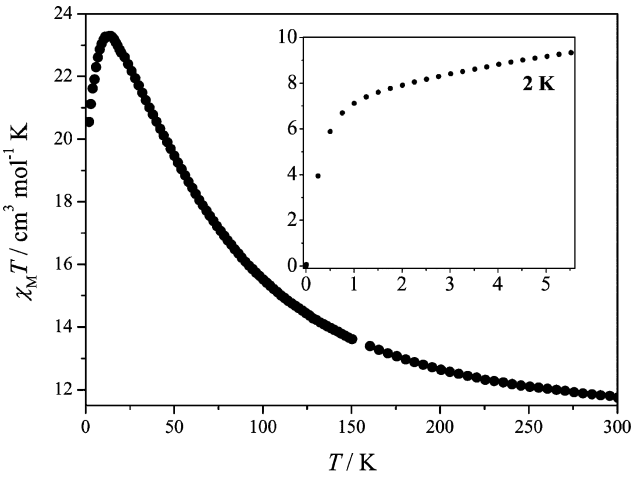

Figure 9. $\chi_M T$ vs T data for complex **2** under a magnetic field of 0.1 T. The inset shows a 2 K magnetization isotherm collected between 0−5.5 T.

assuming $S = 2$ and $g = 2.2$ (Figure 8), further supporting the conclusion of an $S = 2$ ground state.

Magnetic Properties of Complex 2. The magnetic properties of complex **2** show close resemblance to those of complex **IV**, something to be expected considering their structural similarity.

The $\chi_M T$ product for **2** is 11.74 cm^3 mol^{-1} K, significantly higher than the value predicted for four non-interacting $S = 3/2$ ions (7.50 cm^3 mol^{-1} K, $g = 2$). This is partly assigned to the orbital contributions of high-spin Co^{II} ions in octahedral environments, which are known to be important, but also because of the existence of intramolecular ferromagnetic interactions. This latter conclusion is corroborated by the continuous increase of $\chi_M T$ upon cooling, up to a maximum of 23.30 cm^3 mol^{-1} K at 14 K. The decrease below that temperature is attributed to the combined effect of zero-field splitting and Zeeman interactions. However, because of the complications introduced by the orbital contributions of Co^{II} ions, a quantitative treatment of the magnetic susceptibility data of **2** was not attempted. The high-spin ground-state of **2** is illustrated by its magnetization isotherm at 2 K, which shows the onset of saturation above 1 T (Figure 9, inset). Although the saturation is not complete up to 5.5 T, its value is expected to be well over 9 $N_A\mu_B$, indicative of a high-spin ground state.

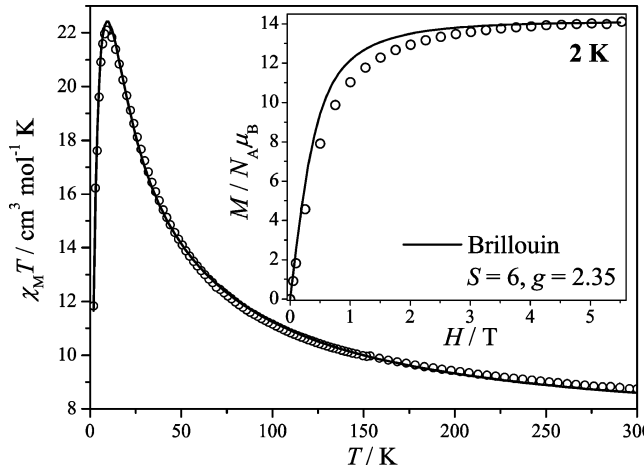

Figure 10. $\chi_M T$ vs T data for complex **3** and the best fit according to the model described in the text. The inset shows a 2 K magnetization isotherm collected between 0−5.5 T. The solid line is a Brillouin curve considering $S = 6$ and $g = 2.35$.

Ferromagnetism in **2** is partly attributed to the magnetic exchange through the end-on azide bridges, which form Co^{II}−N−Co^{II} angles close to 90° (Co(1)−N(21)−Co(2) = Co(1)−N(21)−Co(2″) = 89.156° and Co(2)−N(21)−Co(2″) 105.367°). In addition, the Co^{II}−O-Co^{II} angles, formed by Co^{II} ions and the alkoxo monatomic O-bridge of dpcp, are all 96.484° (because of symmetry). These are also expected to favor the transmission of ferromagnetic exchange between Co^{II} ions.

The high-spin ground-state of **2**, along with the high single-ion anisotropy usually observed for Co^{II} ions in octahedral environments, prompted us to conduct dynamic magnetization experiments to ascertain whether **2** shows magnetic relaxation effects. Variable-frequency and variable-frequency AC magnetic susceptibility experiments carried out down to 2 K showed no out-of-phase signals, thus suggesting the absence of slow magnetic relaxation of **2**.

Magnetic Properties of Complex 3. Magnetic susceptibility data for complex **3** are shown in Figure 10. The $\chi_M T$ product is 8.75 cm^3 mol^{-1} K (1 T), significantly higher than the value predicted for six non-interacting $S = 1$ ions (7.94 cm^3 mol^{-1} K, $g = 2.3$). This is assigned to intramolecular ferromagnetic interactions. This conclusion is corroborated by the increase of the $\chi_M T$ upon cooling, up to a maximum of 22.10 cm^3 mol^{-1} K at 9 K. Upon further cooling, $\chi_M T$ drops abruptly to a value of 11.83 cm^3 mol^{-1} K at 2 K. This decrease is associated with the combined effects of Zeeman splitting inside the magnetic field and zero-field splitting effects experienced by the Ni^{II} ions.

Inspection of the crystal structure of **3** reveals that there are two types of bridging groups between the Ni^{II} ions. One consisting of an alkoxo monatomic O-bridge and one end-on azide, and another consisting of one carbonato monatomic O-bridge and one end-on azide. Considering both cations **3A** and **3B**, we note that in the alkoxo-bridged group, the Ni−O−Ni and Ni−N−Ni angles span the ranges 92.50−94.38° and 91.21−93.85°, respectively, while in carbonato-bridged group they span the ranges 103.69−105.56° and 100.86−102.42°, respectively. This

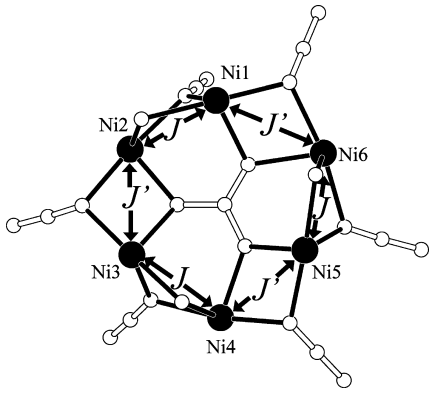

Figure 11. Spin coupling scheme in **3**.

difference may justify the use of two different exchange-coupling parameters, $J_{alkoxo} = J$ and $J_{carbonato} = J'$ (Figure 11). In addition, two different single-ion axial zero-field splitting (zfs) parameters, D and D', may be considered, each corresponding to one of the two Ni^{II} types (see Description of Structures). Finally, a Zeeman term was used to account for the Zeeman splitting inside the magnetic field.

Since introduction of too many parameters could lead to overparametrization of our system, we initially tested a model considering $J = J'$ and $D = D'$. This 1J model could not account for the behavior of **3**, so the first constrain ($J = J'$) was relaxed, leading to a dramatic improvement of our fits. The Hamiltonian used was therefore

$$\hat{H} = -2[J(\hat{\mathbf{S}}_1\hat{\mathbf{S}}_2 + \hat{\mathbf{S}}_3\hat{\mathbf{S}}_4 + \hat{\mathbf{S}}_5\hat{\mathbf{S}}_6) + J'(\hat{\mathbf{S}}_2\hat{\mathbf{S}}_3 + \hat{\mathbf{S}}_4\hat{\mathbf{S}}_5 + \hat{\mathbf{S}}_6\hat{\mathbf{S}}_1)] + D\sum_{i=1}^{6}\hat{S}_{iz}^2 + \beta g\mathbf{H}\sum_{i=1}^{6}\hat{\mathbf{S}}_i \quad (5)$$

Best-fit parameters according to this model were (for $D < 0$) $J = 6.1$ cm^{-1}, $J' = 27$ cm^{-1}, $D = -0.76$ cm^{-1}, $g = 2.18$ with $R = 1.2 \times 10^{-4}$ and (for $D > 0$) $J = 6.1$ cm^{-1}, $J' = 27$ cm^{-1}, $D = 0.89$ cm^{-1}, $g = 2.18$ with $R = 1.2 \times 10^{-4}$ (for the assignment of the exchange parameters see below). The good quality of the fit and the structural resemblance of the two types of Ni^{II} ions did not justify neither the relaxation of the $D = D'$ constrain nor the consideration of additional exchange interactions via the carbonato bridge. The results of these fits reveal an $S = 6$ ground state, separated from the first excited $S = 5$ state by $\sim$18 cm^{-1}. This conclusion was corroborated by isothermal magnetization data collected at 2 K (Figure 10, inset). The experimental data, showing a saturation value close to 14 $N_A\mu_B$, were nicely simulated at high fields by a Brillouin curve considering $S = 6$ and $g = 2.35$. Small discrepancies at low fields are attributed to the small zfs of the ground state.

The uniqueness of this solution was verified by the construction of an error-contour plot of J' versus J, which revealed the presence of two local minima, equivalent because of the symmetry of the problem (Figure 12). The sign of D was not unequivocally established, since the quality of the fits was almost identical for both $D > 0$ and $D < 0$. However, in both cases its magnitude was found to be around 0.8−0.9 cm^{-1}. In both these cases, the energy difference,

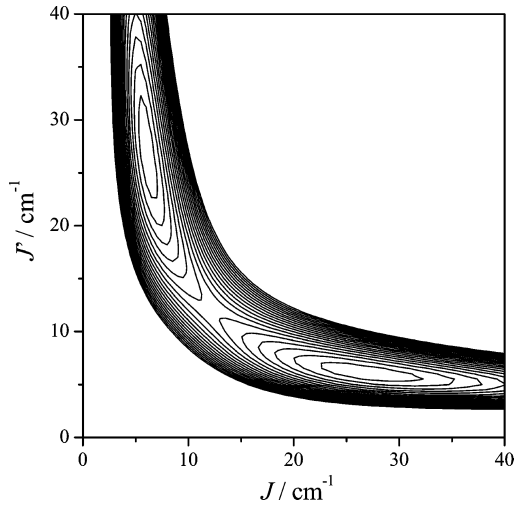

Figure 12. J' vs J error-contour plot showing the two equivalent local minima for fits to the magnetic susceptibility data of **3** with a 2J model ($|D| = 0.8$ cm^{-1}, $g = 2.18$).

ΔE, between the $M_S = 0$ and $M_S = \pm 6$ sublevels, was found to be $\sim 3.25|D|i$. This energy difference is in full agreement with the results derived from the treatment proposed by Gatteschi et al.[27] Assuming N ferromagnetically coupled spins S_i, whose single-ion anisotropy tensors are parallel and have a principal value D_i, the authors propose for the energy difference, ΔE, the relation

$$\Delta E = \frac{2S_i - 1}{2NS_i - 1}N^2S_i^2|D_i| \quad (6)$$

Substituting with $S_i = 1$ and $N = 6$, we find that $\Delta E = (36/11)|D_i| \sim 3.25|D_i|$. If we consider $|D_i| \sim 0.8$ cm^{-1}, as derived from the fits, then $\Delta E \sim 2.6$ cm^{-1}. This gives the measure of the ground-state anisotropy of **3**; assuming that $\Delta E = |D|S^2$ we derive a $|D|$ value of 7×10^{-2} cm^{-1}.

In agreement with the very small D value for the ground state of **3**, variable-temperature and variable-field AC magnetic susceptibility measurements revealed no appreciable out-of-phase signals down to 2 K, thus precluding the possibility of slow magnetic relaxation.

Magnetostructural Correlations. Because of the symmetry of **3** and of the exchange parameters under consideration, the assignment of J and J' is not straightforward; that is, it is not trivial to assign the strongest and weakest ferromagnetic couplings to a particular type of Ni−Ni pairs. Thus, we have to take into consideration the structural characteristics of the bridging moieties in **3** to carry out this assignment. Since magnetic susceptometry is a bulk technique, we require the structural parameters of both **3A** and **3B**. As we previously saw (see Description of Structures) there are two types of Ni−Ni bridged moieties, one containing alkoxo monatomic O-bridges from dpcp, and another containing carbonato monatomic O-bridges from the central CO_3^{2-} anion. Taking those into account, we observe that between the alkoxo-bridged Ni−Ni pairs (considering both

(27) Gatteschi, D.; Sessoli, R.; Villain J. *Molecular Nanomagnets*; Oxford University Press: New York, 2006; pp 46−47.

independent molecules) the average Ni−N−Ni and Ni−O−Ni angles are 92.74 and 93.49°, respectively, while for the carbonato-bridged pairs these angles are 101.84 and 104.42°, respectively.

The studies of Ruiz et al.[25] on the model compound $[Ni_2(\mu\text{-}N_3)_2(NH_3)_8]^{2+}$ determined a maximum ferromagnetic coupling for a Ni−N−Ni angle of 104°, while the model compound $[Ni_2(\mu\text{-}N_3)_3(NH_3)_6]^{+}$ shows a plateau for its maximum ferromagnetic coupling between 90−100° Ni−N−Ni angles. Given that the bridging moieties in our complex differ significantly from the ones considered in Ruiz's models, it is not easy to draw safe conclusions for the exchange-couplings assignment in **3**. However, the former model comprising a double azido bridge can be said to come closer to our Ni−Ni moieties, each of which is bridged by two monatomic bridges (azido/alkoxo and azido/carbonato ones). On the basis of that analogy, we would tentatively propose that the Ni−N−Ni (and Ni−O−Ni) angles closest to 104°, that is, the ones found in the carbonato-bridged Ni−Ni pairs, should be associated with the strongest ferromagnetic couplings. It is noteworthy that the same assignment was decided for complex $\{K\subset[Ni_6(CO_3)(N_3)_6(O_2CMe)_3(dpkMeCN\text{-}H)_3]\}_2[K_2(H_2O)_2]$;[19a] in that case, however, the authors additionally invoked the countercomplementarity effect of *syn-syn* acetates, which they argued should increase the ferromagnetic interaction between azido-bridged Ni^{II} ions. It is also worth mentioning that the derived exchange couplings for that complex ($J = 2.88\ cm^{-1}$, $J' = 25.4\ cm^{-1}$) are very close to those derived for **3**.

Conclusions

From a chemical viewpoint, dpcp continues to prove itself as a source of interesting chemistry in the field of polynuclear transition-metal complexes. In the case of **1**, a new metal core was obtained, containing asymmetric μ_4-azido bridges adopting a $\mu_{1,1,1,1}$ bridging mode. This is particularly interesting, as this bridging mode for azides is very rare, and it is the first time to be observed in a Cu^{II} cluster. On the other side, complex **2** was found to be the close structural analogue of complex **IV**, previously reported by us, their only difference being the replacement of chelating acetates by chelating nitrates. This suggests that the $\{pyC(OMe)(O)pyC(OMe)(O)py\}^{2-}$ form of dpcp in the presence of azides yields a very stable Co^{II}_4 core, present in both complexes **2** and **IV**. The difference in chelates, that is, acetates or nitrates, was shown not to influence the structure of the final product, as both these chelates were nicely accommodated in the two vacant *cis*-coordination sites of the core. This is an important conclusion as it suggests new paths for the Co^{II} chemistry of dpcp. In particular, it suggests the possible use of this metal core as a building block for the preparation of extended structures, connected by *bis*-chelating bridging ligands, which might replace chelating ligands such as acetates or nitrates. We are currently exploring this possibility. A final chemical point of interest is the isolation of complex **3**, containing the singly methanolyzed form of dpcp. This is the second such occurrence of this form of the ligand in our studies, the first being the Ni^{II}_5 complex **V**.[28] Although these examples are not numerous enough to warrant the formulation of a general rule, it should be noted that in the examples studied by us, this form of the ligand was exclusively observed in Ni^{II} clusters.

From a magnetochemical viewpoint, it is shown that dpcp in its solvolyzed forms is a ligand capable of inducing ferromagnetic coupling between Cu^{II} ions because of the near-orthogonality it imposes on their magnetic orbitals. Indeed, complexes **II**, **III**, and **1**, containing dpcp in its hydrolyzed, ethanolyzed, and methanolyzed form, respectively, exhibit ferromagnetic interactions between Cu^{II} ions. In each case, the structural constraints imposed by the ligand induce a near-orthogonality of the magnetic orbitals of bridged Cu^{II} ions, which favors the appearance of ferromagnetic exchange. This conclusion further encourages us to study in greater breadth and depth the Cu^{II}/dpcp reaction system.

Acknowledgment. We are grateful to the Ministerio de Educación y Ciencia (Spain) (Project CTQ2006-15672-C05-03) for its financial support, and FEDER cofinancing.

Supporting Information Available: Crystallographic data in CIF format. This material is available free of charge via the Internet at http://pubs.acs.org. Also, CCDC 713943 (for **1**), CCDC 713944 (for **2**), and CCDC 716235 (for **3**) contain the supplementary crystallographic data for this paper. These data can be obtained free of charge from the Cambridge Crystallographic Data Centre via http://www.ccdc.cam.ac.uk/data_request/cif.

IC900115C

(28) The first occurrence of this form of dpcp was reported in two Cu^{I} complexes in Chen, X.-D.; Mak, T. C. W. *J. Mol. Struct.* **2005**, *748*, 183.